Journal of Physics D: Applied Physics

PAPER • **OPEN ACCESS**

Blade emitters for atmospheric ionic thrusters

To cite this article: M Belan *et al* 2024 *J. Phys. D: Appl. Phys.* **57** 195201

OPEN ACCESS
IOP Publishing
Journal of Physics D: Applied Physics
J. Phys. D: Appl. Phys. **57** (2024) 195201 (11pp)
https://doi.org/10.1088/1361-6463/ad266a

Blade emitters for atmospheric ionic thrusters

M Belan*, **J Baldo, O Kahol and D Montenero**

Politecnico di Milano, Dipartimento di Scienze e Tecnologie Aerospaziali, 20156 Milano, Italy

E-mail: marco.belan@polimi.it

Received 21 September 2023, revised 5 January 2024
Accepted for publication 5 February 2024
Published 14 February 2024

Abstract

In the field of atmospheric ionic thrusters, the objective of this work is to evaluate the possibility of an alternative ionic emitter to the traditional thin wire emitter, in order to overcome the technical issues of the EHD technology related to the fragility of the wires and to make it more suitable to applications outside the laboratory. For the presented experiments, emitters in the form of metallic blades have been produced. These were tested while varying the geometric parameters of both the emitters themselves and of the thruster configuration. Through this measurement campaign, the electrical characteristics, as well as the feasibility and the performances of the new proposed solutions have been evaluated and compared with wire emitters. Results indicate that the blade emitters can work as alternative emitters, however the performance of the present prototypes does not reach that of wire emitters and therefore further research is needed in order to make them a valid alternative.

Keywords: EHD propulsion, atmospheric ion thruster, corona discharge

1. Introduction

Electric propulsion has emerged as a promising trend in aeronautical propulsion, offering potential alternatives to traditional combustion engines [1, 2]. Ionic thrusters in atmosphere, in particular, have gained considerable interest as a viable option because of a good efficiency in terms of thrust-to-power ratio, absence of moving parts, low noise output and low maintenance requirements [3, 4], even if further research is needed to improve their thrust density, which is generally low at present.

In its simplest form, an electrohydrodynamics (EHD) thruster is composed by two electrodes separated by a distance called gap. The ion emitter is typically a thin metallic wire with a diameter generally below 200 μm, the ion collector is, instead, a larger object; often in the shape of a cylinder [5] or an aerodynamic airfoil [6]. A strong electric field is imposed by applying a high voltage difference between the two electrodes through a power source. The intense electric field near the emitter ionizes the gas, initiating a corona discharge. The ions drift towards the collector, transferring their momentum to neutral molecules through collisions. This creates an ionic wind and a net thrust force.

The aforementioned thruster configuration has already been used in flying prototypes such as [6] and a similar one was used by [7]. The majority of EHD thrusters uses thin metallic wires as emitting electrodes; however, these wires are fragile and cannot sustain bending loads. This can potentially lead to an early failure of the system. Increasing the diameter of the wires would increase the robustness of the emitters but, at the same time, it would increase the inception voltage [4], leading to a degradation of the performance of the thruster.

These conflicting requirements indicate that a possible experimental investigation can explore other emitting shapes such as blades or pins which have small curvature radius at their edges, hence facilitating corona inception, but provide much higher structural integrity. The performance of blades and pins emitters has been firstly characterized by a report [3] which also compares it with the one of wire emitters. Additional studies about pin emitters can be found in literature [8–10]. A study of the discharge in blade-to-plate systems can

* Author to whom any correspondence should be addressed.

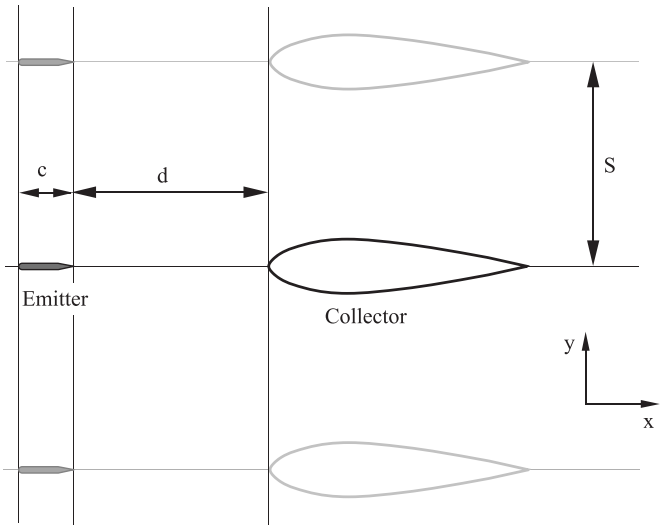

Figure 1. Geometry of an EHD thruster in a multiple propulsion unit configuration.

be found in [11] but it is not oriented towards propulsion. A systematic study about the performance of EHD thrusters using blades as emitters cannot be found in current state of the art literature. The present work focuses on this less studied field and aims to expand upon the embryonic work of [3] and better characterize the behavior of these emitters by independently varying the geometrical parameters described in figure 1. Here the emitters with chord length c are separated from the collectors by the gap d while the distance along the y axis between two propulsive units is the spacing S.

In order to explore the mutual interaction between geometrical parameters, this work considers emitters with a fixed emitting edge and variable chord, tested at different gaps and spacings. All the configurations are compared in terms of current consumption, power consumption, thrust generated and thrust-to-power ratio.

This article is organized as follows: In section 2 the setup and the measurement techniques are presented, including a detailed section 2.3 about the parameters through which the characterization of the blade emitters is accomplished; section 3 presents the results obtained and finally section 4 draws the conclusions.

2. Experimental setup

2.1. Test rig and measurement procedures

The setup employed to perform thrust measurements is depicted in figure 2. The majority of the components has been produced through rapid prototyping, while parts that require high dimensional accuracy have been milled from solid materials.

The collector system consists of up to five parallel airfoils with a span b of 120 mm, fully coated with aluminum and connected to ground. The airfoils ends are protected by insulating caps. In this setup the collectors are airfoils of the National Advisory Committee for Aeronautics (NACA) family, extensively characterized and already used in thrusters which achieved a good performance [6, 12, 13]. In this study, the shape is fixed and corresponds to a NACA0024 airfoil with a chord of 25 mm, as this was shown to maximize the thrust and thrust-to-power coefficients under conditions similar to the present ones and in a wide range of geometrical and electrical parameters [13].

The emitter system consists of up to five parallel metal blades, arranged according to the diagram in figure 1 and connected to the positive pole of the power supply. Each emitter is held in place by two supporting components which also ensure the electrical connection with the high voltage source by means of nylon screws pressing on the contacts. In addition, the supporting components also insulate the ends of the emitter to ensure that the discharge occurs only in the portion of the emitter directly facing the collector. This eliminates ends effects which were shown to degrade the performance of the thruster [7] and the quality of the measurements. These electrodes, which are the object of this investigation, are described in detail in section 2.2 below.

The test rig allows the adjustment of the gap d and the spacing S, as well as the installation of electrodes of different shapes. The number of 5 units (emitter–collector pairs) has been chosen with the aim of approximating periodic properties along the y direction, specifically affected by the spacing parameter S. This number of units is only occasionally reduced for tests requiring very large spacings.

For the thrust measurements, three identical load cells are used, arranged in a radial configuration with equal angular spacing and mounted on a rigid plate. The full scale of each cell is 7.5 N each and the accuracy is ± 1 mN. However, the overall uncertainty in thrust measurements turns out to be larger, ranging from ± 3 mN to ± 5 mN in different tests, because of the mechanical couplings of the system and the error sources. A custom built signal conditioner with high rejection to EM disturbances is used to amplify the mV-range signals of the cells, and all the metal parts of the thrust measurement system are grounded. The thrust T is obtained from the difference $s_{\text{off}} - s_{\text{on}}$ between the load cells output signal when power is switched off and on, using the calibration coefficient of the system k_c:

$$T = k_c \left(s_{\text{off}} - s_{\text{on}} \right) . \tag{1}$$

The coefficient k_c is determined by calibrating the system with a series of different sample weights, and the system response is confirmed as linear by this procedure. The value of k_c turns out to be very stable after repeated checks; it could be affected by large temperature variations, however, as specified below, the experiment is carried out at a stable room temperature. The final thrust values are obtained by multiple measurements in order to ensure repeatability and perform uncertainty estimation.

The electrical components and connections are shown in figure 3. The circuit is powered by a custom made power supply unit (PSU) capable of generating a maximum of 30 kV. The thruster is connected in series to a ballast resistor $R_b = 0.996$ MΩ. The voltage V_a applied to the thruster is measured through a voltage divider with a total resistance of 152.9 MΩ,

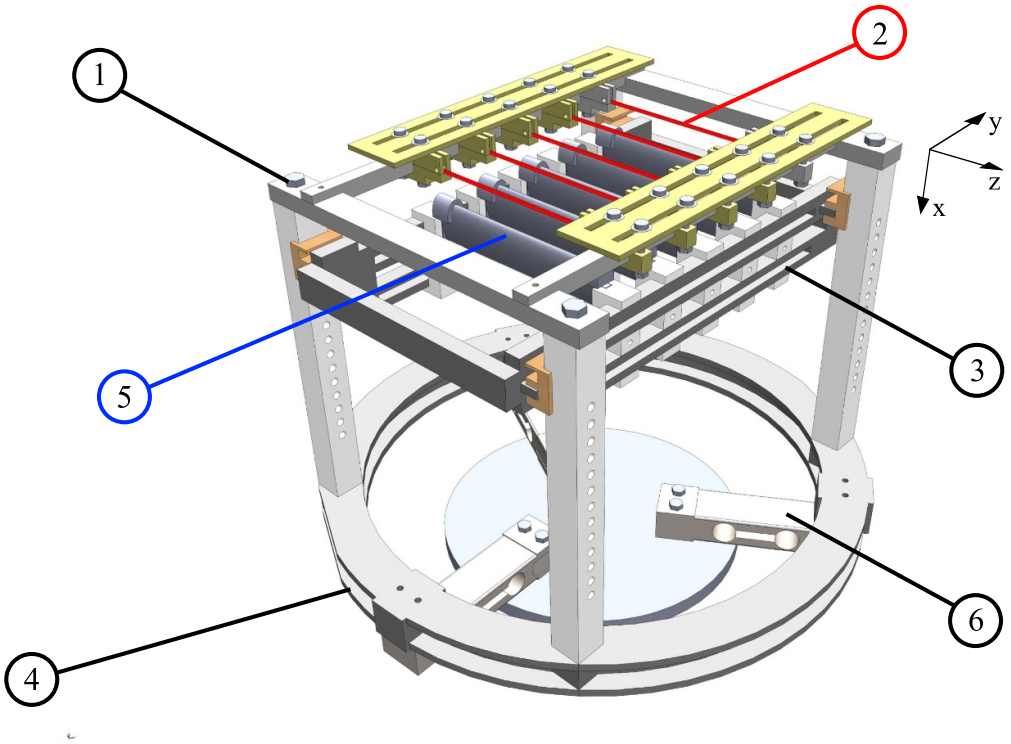

Figure 2. Experimental setup: (1) emitters frame, (2) blade emitters, (3) collectors frame, (4) base ring, (5) airfoil collectors and (6) load cells .

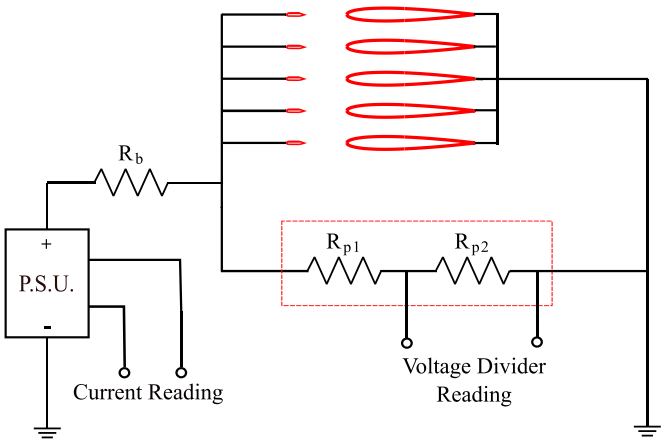

Figure 3. Electric circuit.

with accuracy ± 30 V. The thruster's current consumption I_c is obtained as difference between the total current entering in the circuit from the PSU and the current flowing in the voltage divider's branch. In turn, the total PSU current is measured through a suitable connection based on an internal shunt, with an accuracy of ± 0.01 mA. All signals are acquired by means of a 350 MHz oscilloscope capable of 2.5 GS s^{-1} with 20 M records per trace. The electrical power consumption P_e is obtained by integrating the product of I_c and V_a, accounting for the results of multiple measurements.

The resulting accuracy turns out to be generally better than ± 0.1 W, however in some tests with poor S/N conditions it can worsen to ± 0.2 W as visible in section 3 (for example, in the blue and red curves of figure 9(b)). The ignition voltage V_i is estimated by checking the thruster current I_c, which exhibits for this kind of electrodes a clear and sudden increase with respect to the off conditions, as described in detail in section 3.1 and shown in figure 7.

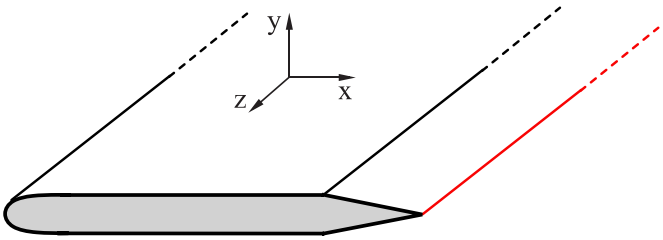

Figure 4. Ideal section of a blade emitter, thickness enlarged for clarity.

All tests were performed in a laboratory environment with a temperature of 20 ± 1 °C and a relative humidity range of 45%–55%.

2.2. Blade emitters

In this work, blade emitters are compared with emitters of very simple technology such as wires, which are manufactured by drawing and are widely available on the market.

The shape of the emitters is sketched in its ideal form in figure 4, oriented with the reference system of figure 1:

- x is the ion drift direction, aligned with the gap.

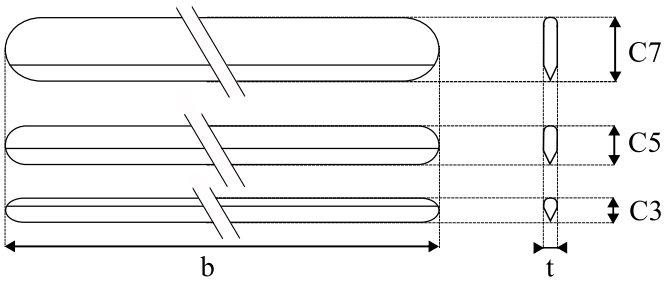

Figure 5. Geometrical parameters of the blade emitters under test. The thickness is not to scale for clarity.

- y is the spacing direction, normal to the lateral surface of the emitter.
- z is the span direction, normal to the emitter cross section.

These blades are made of SK5 steel, with a thickness $t = 800\,\mu$m and have an emitting edge with a curvature radius of $1\,\mu$m, verified by electron microscopy. The final electrodes have been produced through subsequent mechanical machinings which first reduced the chord and then rounded the contour and the edges, so as to obtain the cross-section shown in figure 4 and the plan drawing of figure 5. As explained in detail in section 2.3 below, the length of the chord of the blades greatly affects the performance of the thruster; therefore, three versions of blade emitters, shown in figure 5, have been produced. The span b is fixed and equal to the one of the collectors and the chord has variable length, chosen to be $c = 3, 5$ and 7 mm, and coded as C3, C5, C7.

2.3. Parameter space

The goal of this work is to investigate the performance of an EHD thruster that uses blade emitters as a function of the geometrical parameters, and to ultimately determine whether blade emitters represent a valid alternative to wire emitters. There are, however, technical and scientific challenges that need to be addressed in order to adapt such system to propulsive units.

First and foremost, the phenomenon of multiple emitters unscalability represents the main scientific limit for such thrusters. In fact, in several systems [13–17] it has been observed that increasing the number of the emitters does not lead to a proportional increase in the ionic wind, because an array of emitters at the same potential may create a local region of low potential gradient with detrimental effect on the emitter-collector field, and this effect can be worsened by the hydrodynamic interactions between parallel ionic wind jets. This shielding effect, mathematically described as a deviation from Peek's inception law [18], increases the inception voltage of the emitters. This can happen in an uneven way as some electrodes can be inactive while others are active. Blade emitters, as a result of the large conductive surface area, can enhance this effect, leading to a degradation of the performance of the thruster. To counteract such phenomenon, there is a range of geometrical parameters which can be modified by the designers.

When dealing with studies on the electrodes' geometry, it is important to introduce proper scaling relations in order to identify the physically meaningful parameters and avoid introducing repeated tests which involve similar physics on different scales. This problem has been addressed in different works [12, 13, 19, 20], and it has been shown by [13] that the shielding effect for a given emitter shape is highly dependent on the spacing-to-gap ratio S/d. By increasing the spacing S between emitters or reducing the emitters-collectors gap d their ratio increases and the detrimental electrostatic interaction can be reduced, thereby promoting a better emitter-collector interaction. However, these solutions are not always viable since increasing the spacing would increase the frontal area of the thruster worsening the thrust density, which is an important parameter for the performance [4, 21]. Moreover, decreasing the gap would decrease the thrust-to-power ratio and increase the mass of the final thruster, which depends on the power demand. In this regard, in the literature the range of interest of S/d for some wire–cylinder geometries lies approximately between 0.1–3.5 [19, 22], while for wire–airfoil geometries is between 0.4 and 5 [13, 17, 20]. Optimal values which maximize thrust density can be found, however they may depend on the configuration under study: for airfoil collectors in particular, besides S/d, their chord-to-gap and thickness-to-gap ratios c/d, t/d also affect the performance, so that for different airfoils of the NACA family the optimal S/d ratios appear in a range between 0.5 and 1.5 [20, 23]. For blade–airfoil units these data are not available at all.

The above considerations and some preliminary tests have led to the following parameter ranges in this work. The gap d ranges from 16 to 26 mm, compatibly with the PSU in use and the chosen collectors. The spacing S ranges from 20 to 35 mm with five emitter-collector units; additional tests with larger spacings have been done by setting $S = 70$ mm with three units on the same rig and also with a single unit, which corresponds virtually to $S = \infty$. This leads in turn to an allowed S/d range from 0.77 to 2.19 with five units and larger in the additional tests.

After defining the S/d range, recalling that the span of the emitters was chosen as to match the span of the collectors, the most important free parameter remains the chord c of the emitters, which determines the exposed surface between their parallel sides. In dimensionless form, referring to the gap, this parameter becomes the chord-to-gap ratio c/d. In the present study, preliminary tests with chords ranging up to 25 mm (in the order of the gap) showed that the performance with large chords is poor, thus it is hypothesized that a smaller chord could presumably limit the shielding effect as a smaller surface area can reduce parasitic electrical interactions between emitters. Reducing this parameter could also be beneficial from the aerodynamic point of view since it should reduce the parasitic drag generated by the emitters. Moreover, it would also slightly reduce the weight of the final system since less material can be used and the support structures can be made more

slender and lightweight. It is however clear that machining emitters with a very small chord can be a technical challenge: for instance, for the blade emitters in this work, the heat generated by the mill limited the minimum chord to 3 mm as smaller chords would not dissipate such heat effectively, finally leading to a high risk of damaging the emitting zone.

The considerations above led to a final selection of three chord values from 3 to 7 mm for the presented tests, corresponding to an allowed range of c/d from 0.12 to 0.44, while the preliminary tests indicate that $c/d \sim 1$ or larger is not an interesting range.

A final remark can be added regarding the angle of the emitter tip, which is 11.5°. Like the tip curvature, this parameter is set by the blades manufacturer and cannot be varied in this experiment. It could be considered in further studies, however its asymptotic properties can be inferred in advance: for angles tending to zero, the blade becomes a thin plate, presumably increasing the detrimental effects between parallel electrodes; for very large angles instead the emitters would have blunt tips, favoring arc discharges rather than useful corona discharges.

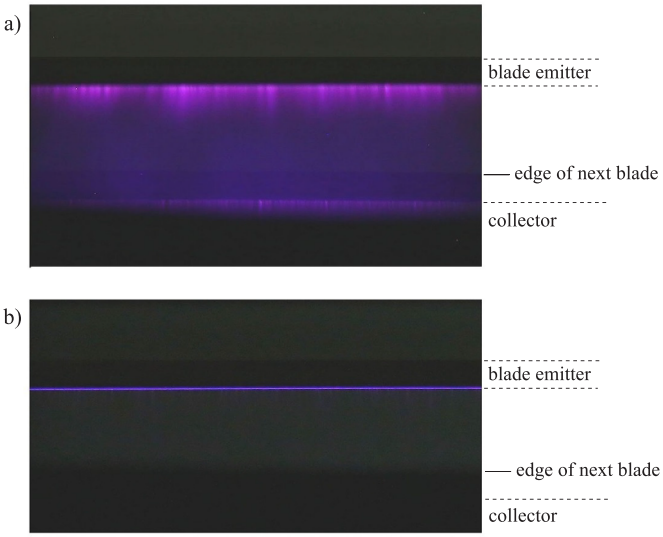

Figure 6. Long exposure images of (a) the initial streamer regime and (b) the corona regime. Due to the orientation of the optical axis, a second blade is visible in the background.

3. Results

3.1. Operating Regimes

The characteristics of the electrical discharge produced by the thruster change with the applied voltage V_a, in a way that can be categorized in different regimes. For progressively rising voltages, these regimes are:

- **Ignition in streamer.** At $V_a = V_i$, the thruster ignites creating a streamer discharge, noisy and clearly visible, as shown in figure 6(a). This regime is also recognizable through the current and voltage signals: actually, the sequence of streamers produces a current signal consisting of repetitive peaks, each one synchronous with a rapid voltage drop across the electrodes. At their appearance, these streamers are quite intense and their peak current is in the order of a few mA, i.e. orders of magnitude larger than the rms noise level (tens of μA), making the identification of the ignition voltage easy. This ignition is different from other known cases, as for example the pin-plate configuration which ignites with weak onset streamers [24, 25]. In this regime the average current remains much lower than the amplitude of the peaks, but at least three times larger than the rms noise level. The thrust generated under these conditions is weak.
- **Intermittent regime.** For higher voltages, an intermittent regime appears, irregularly alternating between the streamer regime and a continuous corona discharge.
- **Corona discharge.** At the end of the transition, a stable and silent corona discharge is formed between the emitters and the collectors. In this regime the emitting region, i.e. the blade edge, appears as a weak glowing line while the entire remaining part of the gap between electrodes, where the ion drift takes place, is dark, as shown in figure 6(b). The behavior of the system in this regime is very similar to the wire-airfoil geometry, where the discharge is dark and only the wire is surrounded by a thin and weak glowing region. The average current is larger than in the streamer regime, and its functional form follows the quadratic relation $I_c \sim V_a^2$, known in literature [4, 24]. This is the optimal operating regime for the thruster, since the generated thrust reaches useful values, thus it will be extensively treated in the results presentation.
- **Breakdown.** At high enough V_a the dielectric strength of air is overcome and strong streamers take place between the emitter and the collector. Under these conditions, a minimum increase in V_a causes sparks between the electrodes. This is the maximum operating voltage of the thruster and it has been encountered in some test only, since the experimental campaign has been run respecting by default the safe operating region of the PSU.

Figure 7 shows a sample sequence of the average current regimes, as a function of the applied voltage. The error bars are reported for the streamer and corona regimes, where statistically stationary mean values and variances can be properly determined, whereas the intermittent regime is inherently less regular.

3.2. Effect of the gap

This section presents the dependence of the operating regime and the performance on the emitters-collectors gap d. For these tests, the emitter chord is fixed at 3 mm and the spacing between units is fixed at 35 mm. The emitter chord is chosen after the considerations of section 2.3, which are confirmed by the results of section 3.4 below. Also the spacing is chosen

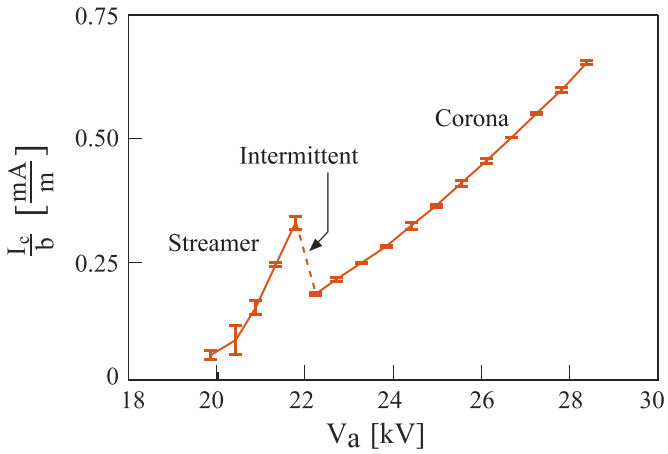

Figure 7. Current curve within different regimes for the blade emitters configuration $c = 5$ mm, $d = 20$ mm, $S = 70$ mm with 1-σ error bars.

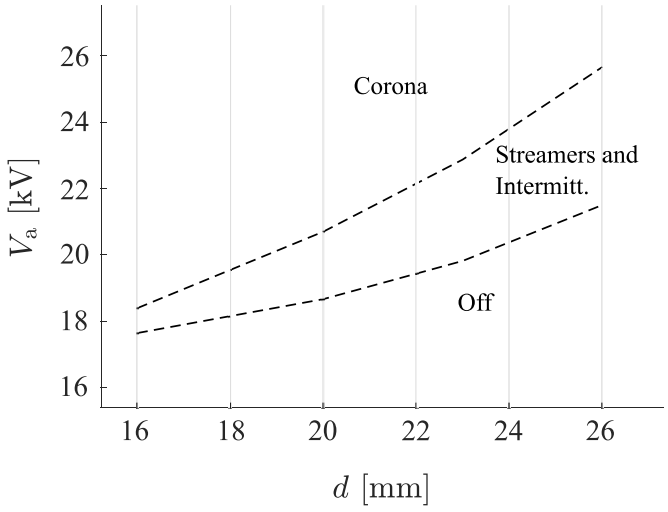

Figure 8. Ignition and corona inception voltage curves as function of the gap d, with $c = 3$ mm and $S = 35$ mm.

following what exposed in section 2.3, taking a large value but avoiding the extreme ones which lead in this setup to reduce the number of thruster units.

Figure 8 shows the values of the ignition and the corona inception voltages as a function of the gap. As this parameter is increased both these voltages increase. The gap length therefore heavily influences the optimal operating range of the thruster, thus posing a strong constraint on the sizing of the electrical structures used. This behavior is to be expected since increasing the gap at constant spacing will favor parasitic interactions between emitters and increase the inception voltage [13, 16]. While the increase of the ignition voltage with the gap is a well known property in literature [24, 25], in the present tests a remarkable result is that also the actual corona inception voltage exhibits the same behavior.

Figure 9 shows current consumption, power, thrust and thrust-to-power ratio for different gaps. Here and in what follows, I_c, P_e and T are always shown per unit span, in order to present results as independent as possible of the specific span length of the present setup. In the corona regime shown in this figure, current, power and thrust all decrease as the gap between the electrodes increases. This is consistent with the existing models [4, 13], which predict that for a given voltage the power and current consumption scale as d^{-2}, while the thrust scales as d^{-1}. On the other hand, the thrust-to-power ratio in the present data increases with the gap; in particular, the data of figure 9(d) can be compared with good agreement to the cited models, where $T/P_e \sim d/V_a$.

3.3. *Effect of the spacing*

This section contains the effects of the units spacing S on the operating regimes and the performance of the thruster. In these tests, the emitter chord is fixed at 3 mm as in the previous tests and the gap is fixed at 20 mm as an intermediate value in the considered range. Owing to the size of the test rig, the thruster consists of five parallel units for spacings S up to 35 mm, then it is reduced to three units for $S = 70$ mm and a single unit is installed to study the behavior of an isolated emitter-collector system, corresponding to $S = \infty$.

Figure 10 shows the values of the ignition and corona inception voltages as a function of the units spacing. Increasing the spacing leads to a decrease for both these values. This is again consistent with the mentioned model [13], since the geometrical dimensionless parameter which controls this behavior is S/d, hence increasing the spacing should have the same effect as decreasing the gap.

More details are shown in figure 11, which summarizes the behavior of the ignition voltage V_i and of the streamer-corona transition voltage as function of the dimensionless spacing, S/d. In particular it shows the curves obtained at constant S and the ones at constant d. All curves indicate that increasing S/d leads to decrease the ignition and transition voltages. The curves at constant S are not equal to the ones at constant d because a change in the gap d modifies all other dimensionless numbers that control the physics of the drift region [13]. Most notably, decreasing the gap also increases the collector thickness-to-gap ratio t/d, facilitating corona inception.

Increasing the units spacing improves all the performance indicators, as shown in figure 12, with the exception of the thrust-to-power which shows a less pronounced dependence. However, the choice of the spacing should be guided by keeping a high surface thrust density $T/(Sb)$, so that in a real design it is preferable to avoid very large spacings and at the same time to reduce the value of the gap in such a way as to obtain a sufficiently high S/d value. In fact, as exposed in section 2.3, a high S/d is preferable because it limits the shielding effect between emitters.

Figure 13 shows the behavior of the thrust density as a function of the applied voltage for different values of the spacing between units (the configuration with $S = \infty$ is not shown as the thrust density vanishes). It confirms that, up to a certain point (in this figure $S = 35$ mm), an increase in the spacing is

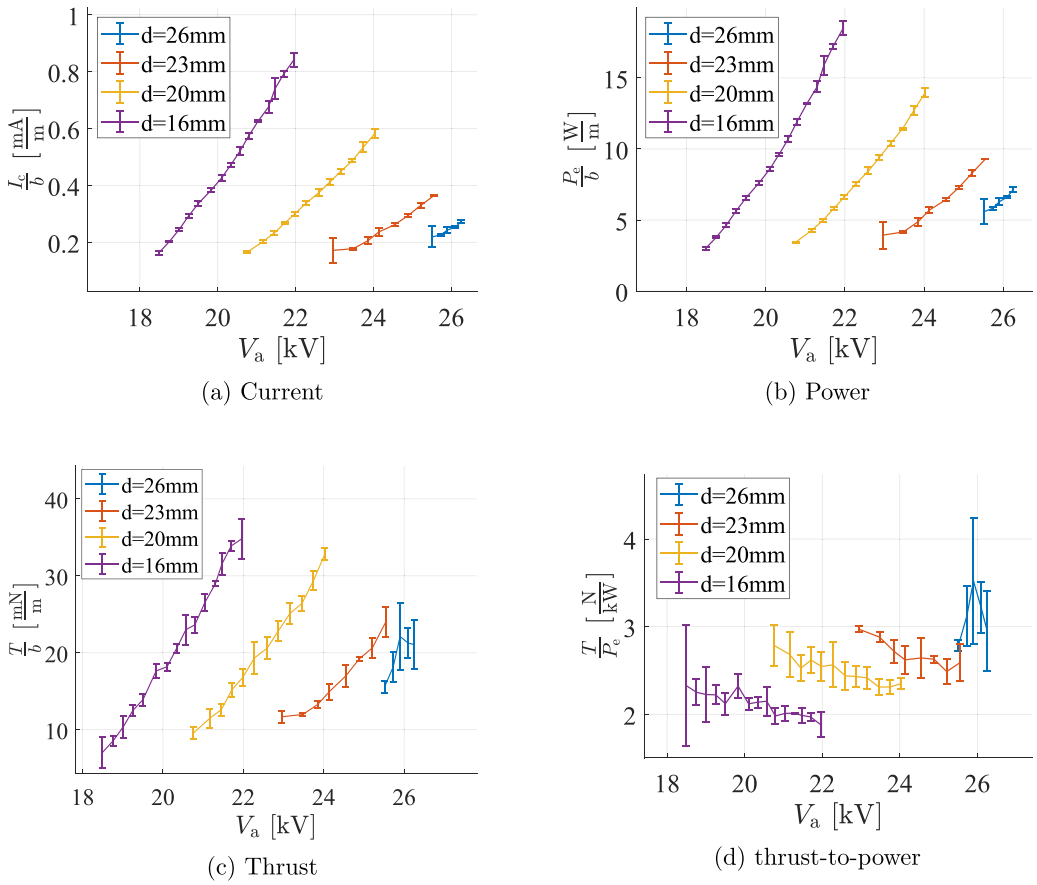

Figure 9. Performance indicators for blade emitters in corona discharge regime as a function of the gap.

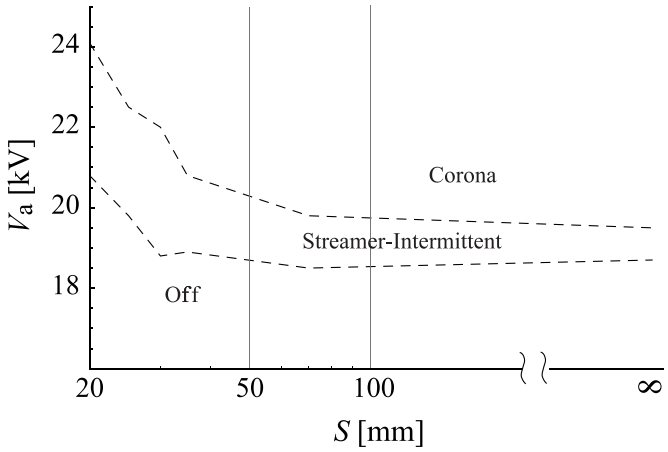

Figure 10. Ignition and corona inception voltage curves as function of the spacing S, with $c = 3$ mm and $d = 20$ mm.

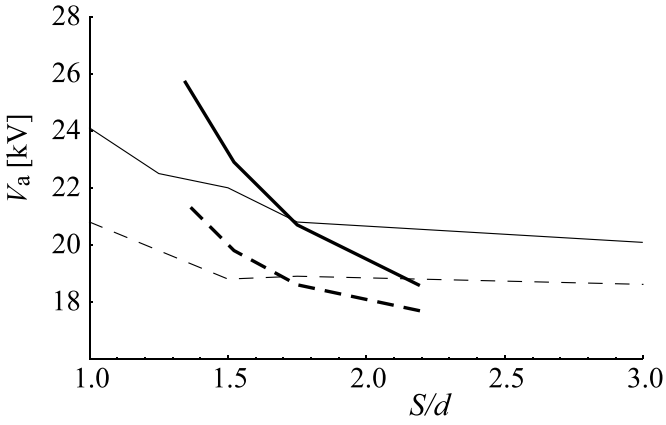

Figure 11. Ignition voltages V_i (dashed lines) and corona inception voltages (solid lines) as function of S/d. Thin lines are for constant d as in figure 10 and thick lines for constant S, from figure 8.

beneficial to the thrust density as it reduces the parasitic interactions between emitters and also the drag between collectors. This effect, however, is not able to compensate the loss in thrust density due to an increase in surface area at large S values and confirms the existence of an optimal spacing as found in other works [19, 23]. For the present case, this value should be identified by refining the investigation in the range $30 < S < 70$ mm.

3.4. *Effect of the chord*

This section reports the effects of the chord parameter on the operating regimes and the performance of the thruster. In these tests, the spacing between units is $S = 35$ mm as in section 3.2 and the gap is fixed at $d = 20$ mm as in section 3.3.

Figure 14 shows the effects of the chord length on the values of ignition voltage and on the voltage ranges of streamer and intermittent regimes. Both the threshold voltages increase

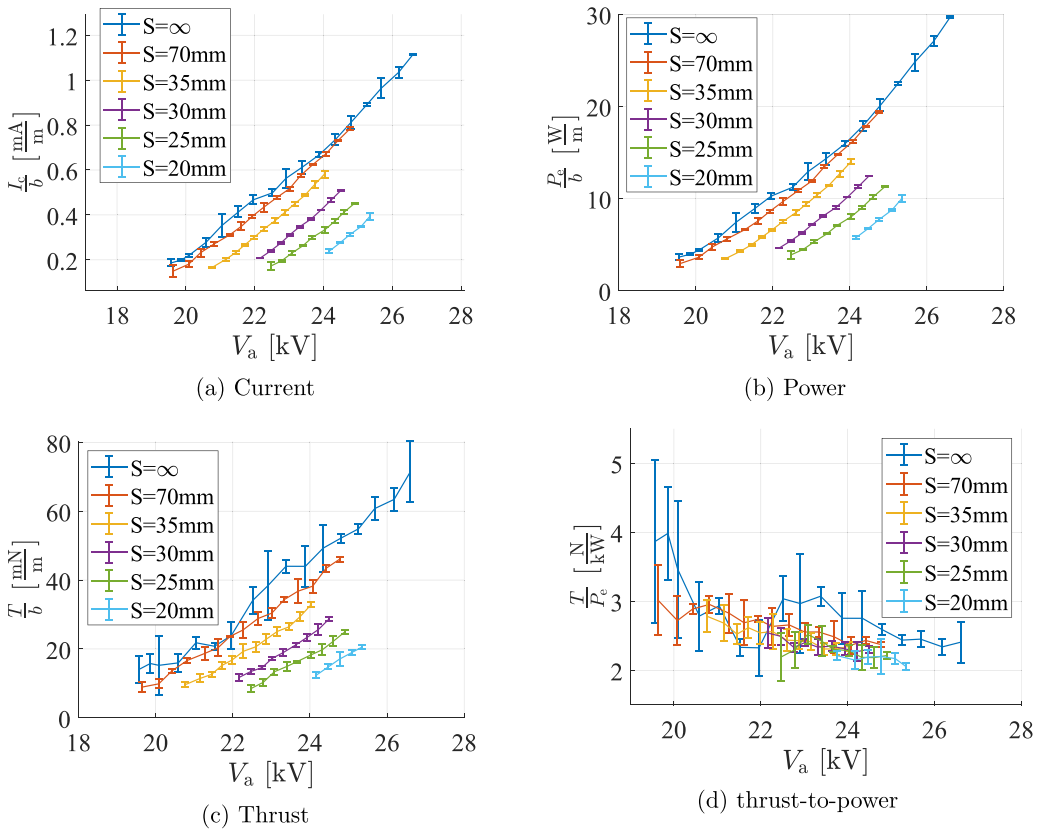

Figure 12. Performance indicators for blade emitters in corona regime as a function of the spacing.

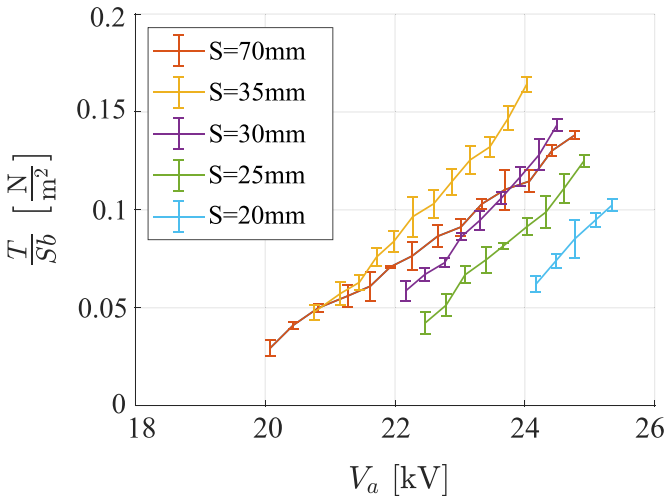

Figure 13. Thrust density for the C3D20 configuration.

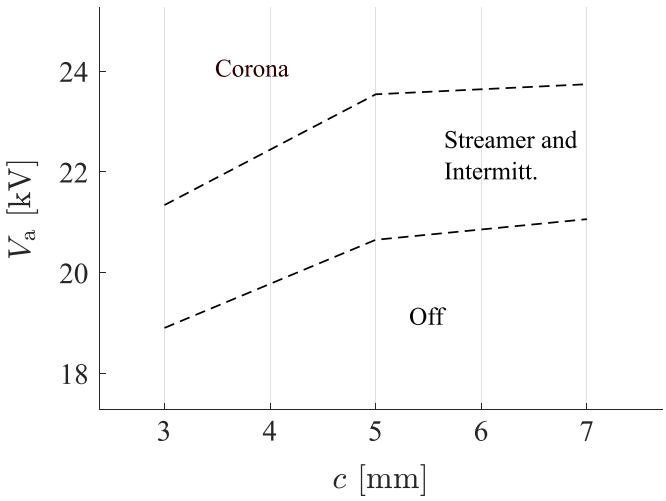

Figure 14. Ignition and corona inception voltage curves as function of the emitters chord c, with $S = 35$ mm and $d = 20$ mm.

with larger chords, indicating a worsening of the electrostatic interaction between emitters. Tests with $c < 3$ mm are not allowed by the technology in use in this work, as exposed in section 2, but the present results lead to hypothesize the benefits of a further decrease of c, i.e. of the lateral area of the emitters, presumably leading to a decrease the ignition voltage.

Figure 15 confirms that decreasing the chord has a beneficial effect on the performance of the thruster, with a major increase when c is reduced from 5 to 3 mm. The net thrust increases significantly while the thrust-to-power shows no significant decrease and, particularly for the higher voltages, variations are small and in the order of the measurement uncertainty. These results indicate that a short chord may help in achieving a high thrust density (which has the same behavior of the thrust for fixed spacing) together with a good thrust-to-power value.

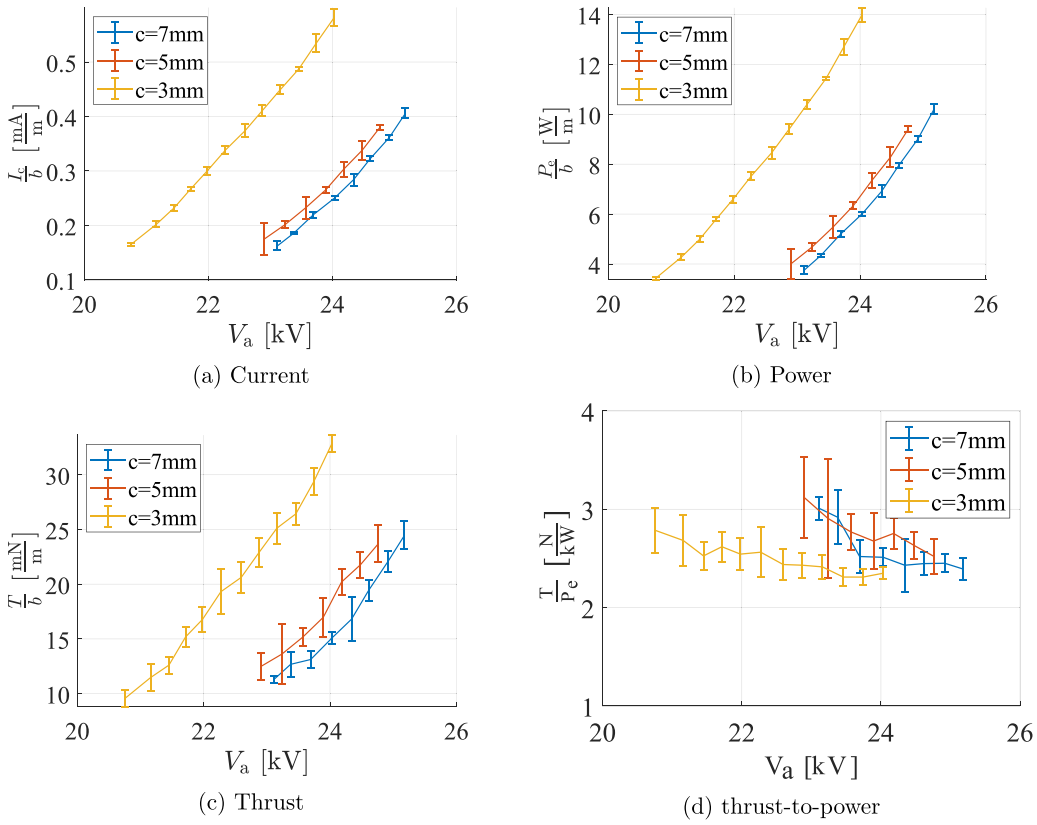

Figure 15. Performance indicators for blade emitters in corona regime as a function of the emitters chord.

3.5. Comparison between blade and wire emitters

This section presents a direct comparison between blade emitters with a chord of 3 mm and wire emitters with a diameter of 30 μm, on the same laboratory setup. The experiments were conducted with a gap $d = 20$ mm and a spacing $S = 35$ mm. The performance indicators are illustrated in figure 16 across a voltage range extending from the corona inception up to values close to the final breakdown, with the appearance of sparks.

Figure 16 shows that even comparing the wires with the best available blades (3 mm chord), wire emitters continue to outperform blade emitters in terms of total thrust generated and thrust-to-power ratio for any given value of the applied voltage (the panel showing I_c vs V_a, closely related to the power plot, is not shown to simplify the discussion). In this figure and in the following one the curves are plotted without error bars in order to better highlight the parameters trends, however for the blade emitters the bars are visible in figure 15 and for the wire emitters the errors are in the order of ± 3 mN m^{-1} for the thrust and ± 0.4 W m^{-1} for the power.

An interpretation of this phenomenon can be given by referring to the dimensionless formulation mentioned above [13]. In that model, the thrust T and the consumed power P_e are made dimensionless, defining the corresponding coefficients C_T, C_P by introducing physically consistent reference values T_{ref} and P_{ref}, as expressed by

$$T = C_T\, T_{\text{ref}} = C_T\, \left(\epsilon_0 V_a^2/d\right) \tag{2}$$

and

$$P_e = C_P\, P_{\text{ref}} = C_P\, \left(\mu_q \epsilon_0 V_a^3/d^2\right)\,, \tag{3}$$

where ϵ_0 is the permittivity and μ_q is the ionic mobility. In turn, the ratio C_T/C_P represents the thrust-to-power ratio coefficient.

The thrust and power curves of figure 16 can be put in dimensionless form by introducing the scaled voltage $\hat{V} = V_a/V_i$, i.e. the ratio between the applied voltage and the ignition voltage. The corresponding curves are depicted in figure 17. This evidences a substantial difference between the two kind of emitters in the considered range, i.e. from corona inception to arcing: in fact, the blades operate substantially close to the condition $\hat{V} \sim 1$ whereas the wires operate over a wide range of $\hat{V}$ values. Following the same model, the behavior of C_T and C_P as functions of $\hat{V}$ can be expressed by asymptotic approximations for small and large $\hat{V}$: in particular, for $\hat{V} \to 1$ (*low voltage limit*) C_T and C_P show a linear dependence on $\hat{V}$, whilst for $\hat{V} \to \infty$ (*high voltage limit*) they take the form $const. + O(\hat{V}^{-1})$, with a slow growth rate tending to saturation.

The results show that wire emitters can operate in both the low and high voltage limits, whereas replacing wires with blades in the same system leads to a low voltage behavior only, and this can be easily shown as a consequence of the high ignition voltage V_i of the blades, which lowers and compresses the values of $\hat{V} = V_a/V_i$ on their curves. In figure 17 the curves do not start exactly at $\hat{V} = 1$ because the wire ignites

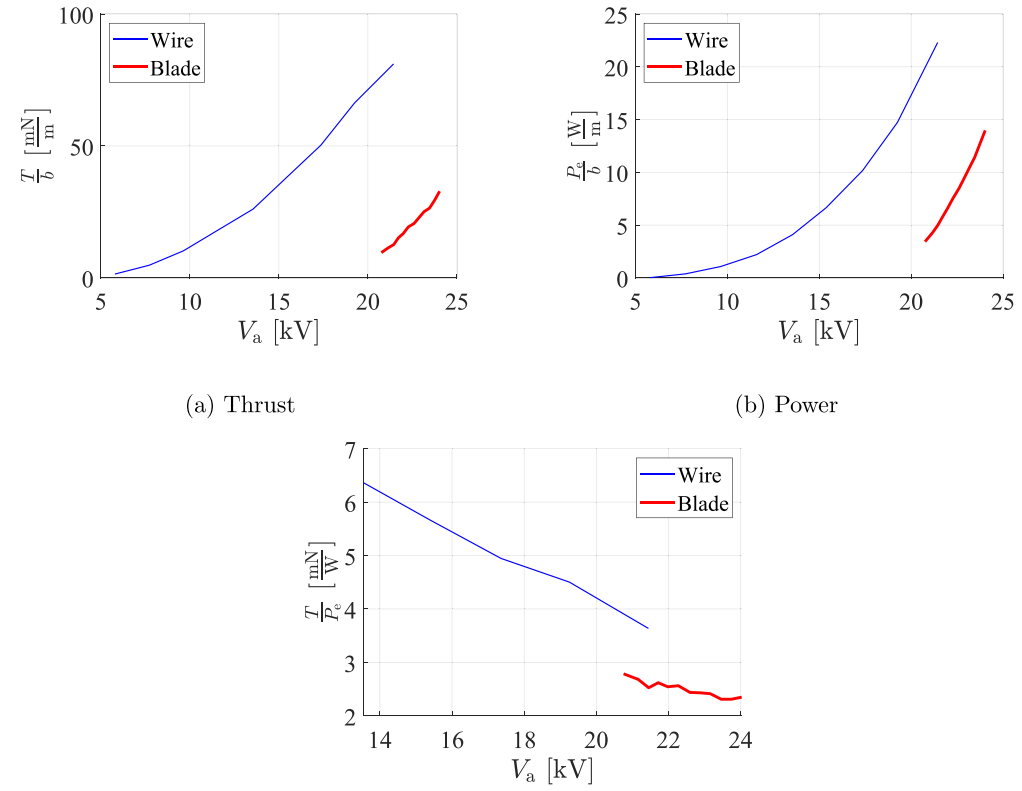

(a) Thrust (b) Power

(c) thrust-to-power

Figure 16. Performance indicators for wire and blade emitters in corona regime.

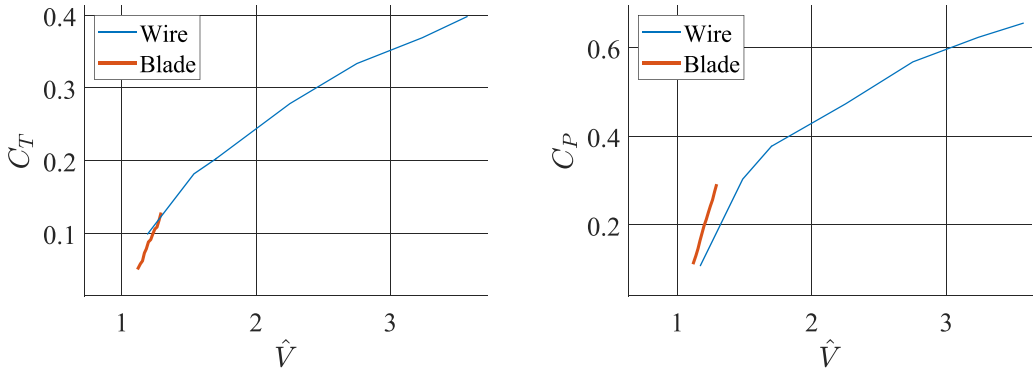

(a) Thrust Coefficient (b) Power Coefficient

Figure 17. Thrust and power coefficient for wire and blade emitters.

in corona regime with very low values of T and P_e, so that the first part of the available data has a large uncertainty; the initial range for the blades instead is not plotted because they ignites in streamer regime and turn to corona regime afterwards. However, the linear trends for low $\hat{V}$ and the saturation behavior for high $\hat{V}$ are clearly visible.

The fact that blade emitters mainly operate in the low voltage limit results in a decrease in the value of every dimensionless coefficient. Additionally, the requirement of a higher applied voltage for their operation significantly diminishes the available thrust-to-power ratio, as the reference value for this ratio is inversely proportional to the ratio of applied voltage to inter-electrode gap. It is worth noting that an hypothetical blade working at higher voltages without arcing and reaching C_T and C_P values similar to the wire would need in dimensional units at least double the voltage of the wire, and would still give very low values of the T/P_e ratio. This points to lowering the ignition voltage V_i as a direction for further research: in turn, this should be related to the curvature radius of the emitting edge and the geometry of the blade. In the present experiments, the emitting radius is much smaller for the blades (1 μm) than for the wires (15 μm), so a plausible explanation for the significantly higher inception voltage of the blades compared to the wires could be attributed to the shielding effect created by the parallel faces of the blades, and not to the curvature radius of the emitting

zones, suggesting further investigations on blades of shorter chords.

4. Conclusions

This work analyzes the performance of blade emitters as a possible alternative to wire emitters for EHD propulsion applications. The blade emitters have been intentionally selected as products of technology as simple as the wires, with an emitting edge defined by the manufacturer. After selecting a definite kind of collectors, the main geometrical parameters turn out to be the gap, the spacing between propulsive units, and the emitter chord, thus a detailed investigation of these parameters is presented.

The study shows that the new emitters with their planar geometry may limit the performance of the thruster, raising the inception voltage and introducing a streamer and an intermittent regime at the ignition of the discharge. Decreasing the conductive surface area of the emitters, by decreasing the chord with mechanical machining, is beneficial to the performance. However, the shortest chord tested was not small enough to bring the blade emitters at the performance level of the wires and lower the ignition voltage to a sufficient extent. Acting on the other geometrical parameters does not improve the performance, as a decrease in the gap or increase in the spacing, although associated with a decrease in the ignition voltage, leads to losses in thrust-to-power and thrust density.

The results obtained with blade emitters were compared to the results obtained with wire emitters under the same conditions. The comparison shows that blade emitters may give performance parameters in the same range of the wires, but generally lower. At present, the higher structural reliability and advantages in installation and maintenance of blade emitters do not appear to compensate the loss in performance.

Further research is required to increase the current understanding of the impact of the ionization region on the generation of thrust, since the wires can emit from the whole surface whereas the blades can only emit from their edge. For small enough wires, their inception voltage follows Peek's law [18] and is proportional to the square root of the emitter's radius. The stiffness of a wire is, on the other hand, proportional to the square of the radius. This indicates that an adequate increase in stiffness can be obtained without suffering a large loss in performance. Instead, the electrodes tested in this work have the characteristic of having a small curvature radius and greater stiffness with respect to wires, but are not yet a viable alternative to wire electrodes. The results of this work indicate that the cause of this loss in performance is due to the large conductive surface area of the blades that negatively influences the inception. Possible future studies can explore improved versions of these electrodes such as micro-blades with a chord smaller than 1 mm which can, potentially, have a stiffness better or comparable to the one of wires of similar thickness but superior performance due to a thinner emitting edge. The minimum interesting chord should remain in this context larger than the diameter of the largest wires in use. That being said, these studies would need to address also issues concerning the manufacturing of these emitters.

Data availability statement

The data cannot be made publicly available upon publication because they are not available in a format that is sufficiently accessible or reusable by other researchers. The data that support the findings of this study are available upon reasonable request from the authors.

ORCID iD

M Belan https://orcid.org/0000-0001-7040-0286

References

[1] Cao W, Mecrow B C, Atkinson G J, Bennett J W and Atkinson D J 2012 *IEEE Trans. Ind. Electron.* **59** 3523–31
[2] Brelje B J and Martins J R 2019 *Prog. Aerosp. Sci.* **104** 1–19
[3] Wilson J, Perkins H and Thompson W 2009 An investigation of ionic wind propulsion *Technical Report* NASA/TM-2009-215822 (NASA)
[4] Masuyama K and Barrett S 2013 *Proc. R. Soc.* A **469** 20120623
[5] Moreau E, Benard N, Lan-Sun-Luk J D and Chabriat J P 2013 *J. Phys. D: Appl. Phys.* **46** 475204
[6] Xu H, He Y, Strobel K, Gilmore C, Kelley S, Hennick C, Sebastian T, Woolston M, Perreault D and Barrett S 2018 *Nature* **563** 532–5
[7] Khomich V and Rebrov I 2018 *J. Electrost.* **95** 1–12
[8] Ieta A and Chirita M 2019 *J. Electrost.* **100** 103352
[9] Drew D and Follmer S 2021 High force density multi-stage electrohydrodynamic jets using folded laser microfabricated electrodes *21st Int. Conf. on Solid-State Sensors, Actuators and Microsystems (Transducers)* (*Inst. of Electrical and Electronics Engineers*) pp 54–57
[10] Chirita M and Ieta A 2022 *J. Propuls. Power* **38** 893–900
[11] Kaci M, Said H A, Laifaoui A, Aissou M, Nouri H and Zebboudj Y 2015 *Braz. J. Phys.* **45** 643–55
[12] Vaddi R, Guan Y, Mamishev A and Novosselov I 2020 *Proc. R. Soc. A: Math. Phys. Eng. Sci.* **476** 20200220
[13] Kahol O, Belan M, Pacchiani M and Montenero D 2023 *J. Electrost.* **123** 103815
[14] Arif S, Branken D J, Everson R C, Neomagus H W J P and Arif A 2018 *J. Electrostat.* **93** 17–30
[15] Islamov R 2020 *J. Electrostat.* **108** 103512
[16] Lemetayer J, Marion C, Fabre D and Plouraboué F 2022 J. Phys. D: Appl. Phys. **55** 185203
[17] Belan M, Terenzi R, Trovato S and Usuelli D 2022 *J. Electrost.* **120** 103767
[18] Peek F 1920 *Dielectric Phenomena in High Voltage Engineering* (McGraw-Hill, Inc.)
[19] Gilmore C and Barrett S 2015 *Proc. R. Soc.* A **471** 20140912
[20] Gomez-Vega N, Brown A, Xu H and Barrett S 2023 *AIAA J.* **61** 767–79
[21] Coseru S, Fabre D and Plouraboué F 2021 *J. Appl. Phys.* **129** 103304
[22] Monrolin N, Plouraboué F and Praud O 2017 *AIAA J.* **55** 4296–305
[23] Belan M, Arosti L, Polatti R, Maggi F, Fiorini S and Sottovia F 2021 *J. Electrost.* **113** 103616
[24] Kuffel E, Zaengl W and Kuffel J 2000 *Electrical Breakdown in Gases* (*High Voltage Engineering Fundamentals*) 2nd edn (Newnes) ch 5, pp 281–366
[25] Fridman A and Kennedy L 2004 *Plasma Physics and Engineering* (Taylor & Francis)